most weakly coupled QDs is as low as the spectral resolution of our spectrometer, 40 μeV, a value comparable to the smallest linewidth reported so far (6). The decrease of the exciton lifetime for the antibonding state with increasing level separation can be described in a simple two-level picture involving acoustical phonon scattering from the upper state into the lower state (19). This would lead to a cubic dependence of this linewidth on the energy level separation, which is also observed experimentally.

CEO has proven to be a versatile method for the fabrication of zero-dimensional objects of well-defined size, shape, and position. The excellent optical quality, manifested in extremely narrow emission lines, and the high degree of homogeneity accessible with this method permit the precise tailoring of the quantum-mechanical coupling between these nanoscale structures. As an extension to this work, we propose the use of higher barriers, narrower QWs, and the incorporation of indium into the wells. All these measures should increase the binding energy of excitons to the QDs. The use of strained InGaAs QWs, in particular, is expected to enhance this binding energy drastically because the strain can be almost completely elastically relaxed at the intersections. This might open a route to experimental investigation of a variety of quantum mechanics textbook examples previously inaccessible by other means, such as going from artificial atoms to molecules to an artificial one-dimensional solid.

REFERENCES AND NOTES

1. K. Brunner *et al.*, *Phys. Rev. Lett.* **69**, 3216 (1992).
2. N. C. van der Vaart *et al.*, *ibid.* **74**, 4702 (1995); F. R. Waugh *et al.*, *ibid.* **75**, 705 (1995).
3. A. Zrenner *et al.*, *ibid.* **72**, 3382 (1994).
4. H. F. Hess, E. Betzig, T. D. Harris, L. N. Pfeiffer, K. W. West, *Science* **264**, 1740 (1994).
5. K. Brunner, G. Abstreiter, G. Böhm, G. Tränkle, G. Weimann, *Phys. Rev. Lett.* **73**, 1138 (1994).
6. D. Gammon, E. S. Snow, B. V. Shanabrook, D. S. Kratzer, D. Park, *ibid.* **76**, 3005 (1996); *Science* **273**, 87 (1996).
7. J.-Y. Marzin, J.-M. Gérard, A. Izraël, D. Barrier, G. Bastard, *Phys. Rev. Lett.* **73**, 716 (1994).
8. R. Leon, P. M. Petroff, D. Leonard, S. Fafard, *Science* **267**, 1966 (1995).
9. M. Grundmann *et al.*, *Phys. Rev. Lett.* **74**, 4043 (1995).
10. M. A. Kastner, *Phys. Today* **46**, 24 (January 1993); O. Klein *et al.*, *Phys. Rev. Lett.* **74**, 785 (1995); R. C. Ashoori *et al.*, *ibid.* **71**, 613 (1993); R. C. Ashoori, *Nature* **379**, 413 (1996).
11. S. Tarucha, D. G. Austing, T. Honda, R. J. van der Hage, L. P. Kouwenhoven, *Phys. Rev. Lett.* **77**, 3613 (1996).
12. Y. Arakawa and A. Yariv, *IEEE J. Quantum Electron.* **22**, 1887 (1986).
13. L. Kouwenhoven, *Science* **268**, 1440 (1995).
14. L. Pfeiffer *et al.*, *Appl. Phys. Lett.* **56**, 1697 (1990).
15. Light from a tunable dye laser was focused through a microscope objective lens (numerical aperture = 0.75, power density = 50 W cm^{-2}) onto the sample mounted in a He cryostat. Under such conditions, less than one exciton at a time is expected to be in the QDs. The emitted light was collected by the same objective lens and directed to a confocal imaging system, which defined a nearly diffraction-limited detection range of FWHM = 800 nm. The PL signal was dispersed with a triple-grating spectrometer (spectral resolution = 40 μeV) and detected with a cooled charge-coupled-device camera.
16. The PL energy of (110) QWs is red-shifted with respect to that of (001) QWs of identical thickness because of different heavy hole masses in these two directions.
17. J. Hasen *et al.*, *Nature* **390**, 54 (1997).
18. M. Grundmann and D. Bimberg, *Phys. Rev. B* **55**, 4054 (1997).
19. P. Platzman, personal communication.
20. Y. C. Chang, L. L. Chang, L. Esaki, *Appl. Phys. Lett.* **47**, 1324 (1985).
21. A. R. Göni *et al.*, *ibid.* **61**, 1956 (1992).
22. W. Wegscheider *et al.*, *Phys. Rev. Lett.* **71**, 4071 (1993).
23. T. Someya, H. Akiyama, H. Sakaki, *ibid.* **74**, 3664 (1995); *ibid.* **76**, 2965 (1996).
24. W. Wegscheider, G. Schedelbeck, G. Abstreiter, M. Rother, M. Bichler, *ibid.* **79**, 1917 (1997).

25. We thank A. Zrenner for helpful discussions. Supported by the Deutsche Forschungsgemeinschaft in the framework of SFB 348 and the Bundesministerium für Bildung, Wissenschaft, Forschung, und Technologie through contract 01 BM 630/1.

13 August 1997; accepted 15 October 1997

Organically Modified Aluminosilicate Mesostructures from Block Copolymer Phases

Markus Templin, Achim Franck, Alexander Du Chesne, Heike Leist, Yuanming Zhang, Ralph Ulrich, Volker Schädler, Ulrich Wiesner*

Organically modified aluminosilicate mesostructures were synthesized from two metal alkoxides with the use of poly(isoprene-*b*-ethyleneoxide) block copolymers (PI-b-PEO) as the structure-directing molecules. By increasing the fraction of the inorganic precursors with respect to the polymer, morphologies expected from the phase diagrams of diblock copolymers were obtained. The length scale of the microstructures and the state of alignment were varied using concepts known from the study of block copolymers. These results suggest that the use of higher molecular weight block copolymer mesophases instead of conventional low–molecular weight surfactants may provide a simple, easily controlled pathway for the preparation of various silica-type mesostructures that extends the accessible length scale of these structures by about an order of magnitude.

Currently, a great deal of attention is being paid to the synthesis of complex inorganic materials with long-range order (1). Such materials could find applications in catalysis, membrane and separation technology, and molecular engineering (2). A typical approach is the use of organic structures formed through self-assembly as structure-directing agents. The final morphology is then determined by the cooperative organization of inorganic and organic molecular species into three-dimensionally structured arrays, a concept also discussed in the context of biomineralization (3). This strategy has already been successfully used in the preparation of inorganic mesoporous materials (4). Different pathways, where the driving forces of the cooperative organization are either ionic (5) or based on hydrogen bonds (6), have been described in vastly different concentration regimes (7). Pore sizes of 20 to 100 Å are commonly obtained in this way.

Here, we used block copolymers of higher molecular weight to make the transition from the small to the large mesoscopic regime (up to several tens of nanometers) of silica-type mesostructures. Bagshaw *et al.* previously used block-type low–molecular weight surfactants as templating agents to produce mesoporous molecular sieves (6). Higher molecular weight block copolymers have been used to stabilize inorganic metal or semiconductor nanoparticles (8). However, they all produce solid particles with morphologies never very far from spherical (9). An example of a different shape of inorganic material in a random-coil organic homopolymer is the synthesis of randomly distributed inorganic nanowires (10). Most recently, block copolymers have been used to control the growth of anisotropic inorganic crystals (11).

Block copolymer materials are similar to low–molecular weight nonionic surfactant solutions with respect to their general phase behavior (12). The phase diagrams of these materials have been elucidated by numerous experimental and theoretical studies (13). The combination of inorganic siliceous components in a hybrid material with block copolymers is appealing for various reasons.

Max-Planck-Institut für Polymerforschung, Postfach 3148, 55021 Mainz, Germany.

*To whom correspondence should be addressed.

First, a blend of desirable macroscopic properties (mechanical, thermal, and so forth) in the final product can be expected. Because the block copolymer chemistry (architecture, chain length, composition, and so forth) can be varied substantially, it should be possible to fine tune the properties of the composite. Moreover, the length scale of the microstructures of block copolymers is on the order of the characteristic length scale of the chains, ranging from 5 to 100 nm, which may make mesoporous materials with large pore sizes accessible. We investigated the sol-gel process of a mixture of two metal alkoxides, (3-glycidyloxypropyl-)trimethoxysilane, $(CH_3O)_3Si(CH_2)_3OCH_2\overline{CHCH_2O}$ (GLYMO), and aluminum *sec*-butoxide, $Al(OBu^s)_3$, with poly(isoprene-*b*-ethyleneoxide) block copolymers (PI-b-PEO) (Fig. 1). GLYMO itself is an interesting hybrid material known to form thin-film coatings on polymers, thereby enhancing the abrasion resistance up to values of conventional glass (*14*). The block copolymer has two important features. First, the hydrolysis products of the metal alkoxides should preferentially swell the hydrophilic PEO block as a result of hydrogen bonding (as known, for example, from the synthesis of mesoporous molecular sieves with low–molecular weight nonionic surfactants) (*6*, *7*). Second, the low glass transition temperature $T_g \approx 213$ K of the PI block introduces high mobility at ambient temperatures and should allow rapid formation of structures with long-range order even in the bulk.

Two PI-b-PEO block copolymers, referred to as PP3 and PP7, were synthesized by anionic polymerization using a recently described procedure (*15*). The molecular weights are nearly 10 kg mol^{-1} (PP3) and 34 kg mol^{-1} (PP7), and the polydispersity is low ($\overline{M}_w/\overline{M}_n \approx 1.05$, where $\overline{M}_w$ and $\overline{M}_n$ are the weight-average and number-average molecular weights, respectively). The volume fraction of the PEO block is ~15% in both cases. Their microdomain structure was explored by small-angle x-ray scattering (SAXS) (Fig. 2). In a representative SAXS pattern obtained for PP3 at room temperature (Fig. 2A), the main peak is centered around a value for the scattering wave vector q corresponding to ~11.9 nm. There are at least two higher order reflections clearly visible at angular positions of $\sqrt{2}$ and $\sqrt{3}$ of the first-order maximum. This pattern is characteristic for spheres packed in a simple or body-centered cubic lattice, as expected for this volume fraction.

In a typical preparation of an organic-inorganic composite, 0.5 g of PI-b-PEO block copolymer was dissolved in a 1:1 mixture of $CHCl_3$ and tetrahydrofuran (5 weight % polymer); under moderate stirring, a prehydrolyzed solution of 80 mol % GLYMO and 20 mol % $Al(OBu^s)_3$ (*16*) was added, and after 2 hours the mixture was transferred to a petri dish at 333 to 343 K. After subsequent evaporation of the organic solvents (~1 hour), the formation of the composite was accomplished by heat treatment at 403 K in vacuum for 45 min. A series of film samples with thicknesses of ~0.5 to 1 mm were prepared in this way by adding different amounts of the metal alkoxide solution to the same block copolymer. In the following, we focus on samples with 0.22 and 0.57 g of metal oxides in 0.5 g of PP3, denoted PP3/4 and PP3/10, respectively.

In the SAXS pattern of PP3/4 (Fig. 2B), the main peak is located at a q value corresponding to ~20.3 nm, and there are higher order reflections at angular positions of $\sqrt{4}$ and $\sqrt{7}$ of this first-order maximum. This spacing sequence is indicative of a hexagonal array of cylinders. For PP3/10 (Fig. 2C), the main peak is centered around a q value corresponding to ~19.6 nm, and two more reflections of higher order are clearly visible at integer multiples of this q value. Such a sequence is characteristic of an arrangement of lamellae.

To corroborate the assignment of these two SAXS patterns to a cylindrical and a lamellar morphology, respectively, we also examined the samples by transmission electron microscopy (TEM) (Fig. 3). The contrast in these micrographs arises from PI, stained with OsO_4 and appearing black. The image of PP3/4 (Fig. 3A) clearly shows hexagonally packed cylinders in the two most typical projections. The TEM image of PP3/10 (Fig. 3B) exhibits lamellae. To determine whether the silica-type material is confined to one phase of the block copolymer, we used the recently developed method of elemental mapping (*17*). In Fig. 3C the silicon map of the same area depicted in Fig. 3B is shown; areas containing silicon appear bright in this image. Two conclusions can be drawn from Fig. 3C: (i) The inorganic silicon-rich phase

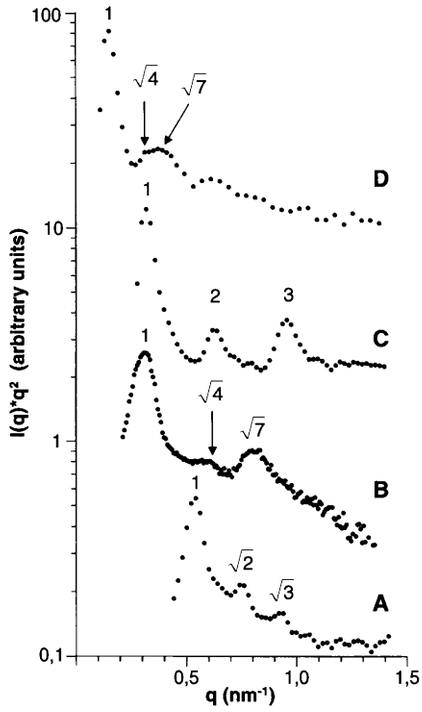

Fig. 2. Scattered intensities $I(q)$ as a function of scattering vector q for PP3 (**A**), PP3/4 (**B**), PP3/10 (**C**), and PP7/4 (**D**) at 295 K. Angular positions of higher order peaks with respect to the first-order maximum are indicated for each curve. The maxima with an angular position of $\sqrt{3}$, usually expected for a cylindrical morphology, are not well resolved in curves (B) and (D), probably because of the large width of the peaks. The patterns in (A), (C), and (D) were obtained with a Kratky compact camera (Anton Paar KG) equipped with a one-dimensional position-sensitive detector (M. Braun). The Ni-filtered Cu Kα radiation (λ = 0.154 nm) was from a Siemens generator (Kristalloflex 710 H) operating at 35 kV and 30 mA. The pattern in (B) was obtained with a Rigaku Rotaflex x-ray source and a 2D area detector after integration over the azimuthal angle (see Fig. 4).

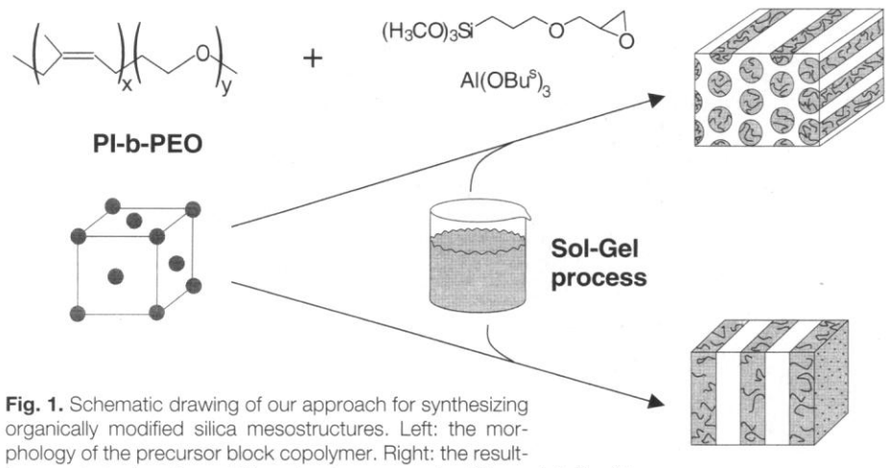

Fig. 1. Schematic drawing of our approach for synthesizing organically modified silica mesostructures. Left: the morphology of the precursor block copolymer. Right: the resulting morphologies after addition of various amounts of the metal alkoxides.

has a lamellar morphology, and (ii) comparison of Fig. 3B and Fig. 3C shows that silicon is confined to the PEO phase of PP3. The same spatial distribution can be shown by aluminum mapping, and similar results were obtained for the hexagonal phase (*18*).

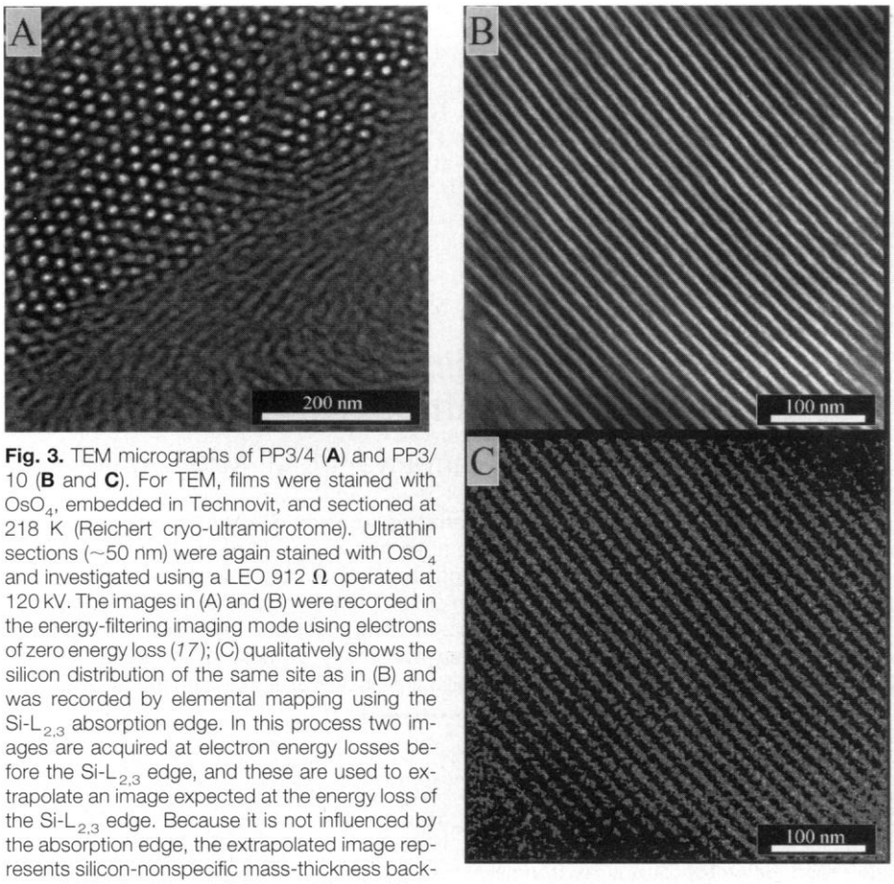

Fig. 3. TEM micrographs of PP3/4 (**A**) and PP3/10 (**B** and **C**). For TEM, films were stained with OsO_4, embedded in Technovit, and sectioned at 218 K (Reichert cryo-ultramicrotome). Ultrathin sections (~50 nm) were again stained with OsO_4 and investigated using a LEO 912 Ω operated at 120 kV. The images in (A) and (B) were recorded in the energy-filtering imaging mode using electrons of zero energy loss (*17*); (C) qualitatively shows the silicon distribution of the same site as in (B) and was recorded by elemental mapping using the Si-$L_{2,3}$ absorption edge. In this process two images are acquired at electron energy losses before the Si-$L_{2,3}$ edge, and these are used to extrapolate an image expected at the energy loss of the Si-$L_{2,3}$ edge. Because it is not influenced by the absorption edge, the extrapolated image represents silicon-nonspecific mass-thickness background. This background is then subtracted from a third image acquired at the Si-$L_{2,3}$ edge, the difference image representing the pure distribution of silicon to the contrast (*24*). The smaller distance in the lamellar spacing in the TEM images relative to that indicated by the SAXS data is a result of contraction of the ultrathin sections normal to the plane of the lamellae, driven by free energy minimization (*25*).

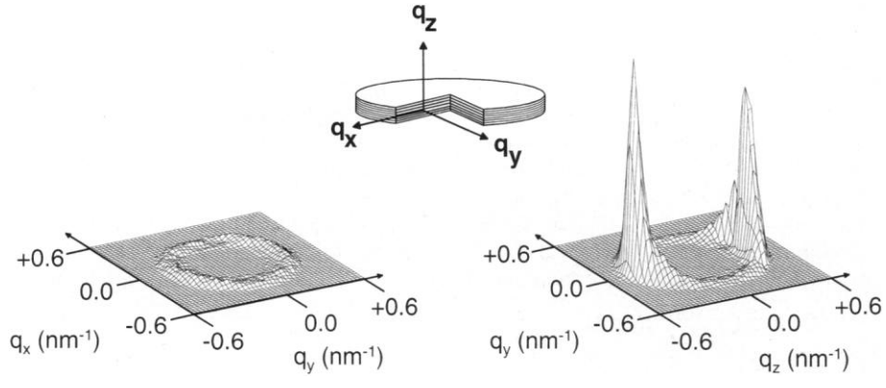

Fig. 4. Two-dimensional SAXS patterns of PP3/10 at 295 K for two different directions of the x-ray beam with respect to the sample coordinate frame, as schematically depicted in the inset. The order parameter $\langle P_2 \rangle$ for the angular distribution of the lamellae normal with respect to the *z*-direction (film-normal), as obtained from the 2D SAXS pattern (*21*) on the right side, is 0.5. Patterns were obtained with a Rigaku Rotaflex x-ray source at 0.154 nm (Cu Kα). A three-pinhole collimator was used to generate a beam 1 mm in diameter. Scattering patterns were recorded on a 2D Siemens X-1000 area detector with a sample-to-detector distance of 130 cm.

The length scale of the morphologies in the present composites reflected from the SAXS patterns in Fig. 2, B and C, is ~20 nm, considerably longer than what is typically obtained for materials prepared from low–molecular weight surfactants. The spacings can be further increased by using higher molecular weight block copolymers. In composites prepared from PP7, spacings of ~40 nm were achieved (Fig. 2D). Because molecular weights of up to 10^2 to 10^3 kg mol^{-1} can be synthesized, fine-tuning of morphological parameters becomes possible.

The electron microscopy results (Fig. 3) suggest that the hydrophilic PEO block acts as an anchor for the metal alkoxide condensation products. More information about this effect was obtained from differential scanning calorimetry (DSC) (*19*). Although the T_g value of the PI block is unaffected, the melting behavior of the PEO block is markedly altered by the addition of inorganic material (*18*). For pure PP3, a melting point T_m was clearly detected at 310 K. For samples PP3/4 and PP3/10, however, the crystallization of the PEO block was suppressed. This is a well-known phenomenon in polymer blending, where the intimate mixing of a second polymer prevents PEO crystallization (*20*). Crystallization is only suppressed, however, if during the synthesis the organic solvents are evaporated at temperatures above the T_m of PEO. This suggests that the PEO chains and the hydrolysis products of the metal alkoxides mix well only above the T_m of the PEO block, and this state is frozen through condensation of the metal alkoxides.

Information about the inorganic connectivities can be gained by solid-state nuclear magnetic resonance. The condensation behavior of the present mixtures is similar to that of the pure metal alkoxides (*21*). Most of the silicon atoms are connected to two or three other metal atoms (silicon or aluminum) by oxygen bridges, thereby yielding a three-dimensional network. Nearly 40% of the aluminum is incorporated in this network as fourfold coordinated species. The residual aluminum is located in aluminum oxohydroxo complexes, $AlO_x(OH)_y(H_2O)_z$, as sixfold coordinated aluminum. In addition to the links on the inorganic side, the conversion of the epoxy group to oligoethyleneoxide derivatives leads to a higher network density.

Finally, we concentrate on orientational effects induced by the solvent-cast technique (*22*), which is part of the preparation procedure for our materials. Two-dimensional (2D) SAXS patterns for two different orientations of a film of lamellar sample PP3/10 with respect to the x-ray beam (Fig. 4) show that in the q_x-q_y plane (film plane) only a ring of small scattering intensity is

observed, whereas in the q_y-q_z plane two strong and narrow scattering peaks along q_z are detected. This result is expected for lamellae oriented parallel to the film surface. It demonstrates that the solvent-cast technique is capable of inducing macroscopically aligned samples for the present lamellar silica-type mesostructures. Because the film thickness of these materials is considerable (~1 mm), surface-induced morphological transitions and related effects observed for very thin films (*23*) can be neglected.

REFERENCES AND NOTES

1. M. Antonietti and C. Göltner, *Angew. Chem.* **109**, 944 (1997); S. Mann and G. Ozin, *Nature* **382**, 313 (1996); P. Behrens, *Adv. Mater.* **5**, 127 (1993).
2. L. Mercier and T. J. Pinnavaia, *Adv. Mater.* **9**, 500 (1997); F. Schüth, *Ber. Bunsenges. Phys. Chem.* **99**, 1306 (1995).
3. S. Mann, *Nature* **365**, 499 (1993); B. R. Heywood and S. Mann, *Adv. Mater.* **6**, 9 (1994).
4. C. T. Kresge, M. E. Leonowicz, W. J. Roth, J. C. Vartuli, J. S. Beck, *Nature* **359**, 710 (1992); N. K. Raman, M. T. Anderson, C. J. Brinker, *Chem. Mater.* **8**, 1682 (1996).
5. Q. Huo *et al.*, *Nature* **368**, 317 (1994); Q. Huo, D. I. Margolese, G. D. Stucky, *Chem. Mater.* **8**, 1147 (1996); Q. Huo, R. Leon, P. M. Petroff, G. D. Stucky, *Science* **268**, 1324 (1995); A. Firouzi *et al.*, *ibid.* **267**, 1138 (1995).
6. S. A. Bagshaw, E. Prouzet, T. J. Pinnavaia, *Science* **269**, 1242 (1995).
7. A. Firouzi, F. Atef, A. G. Oertli, G. D. Stucky, B. F. Chmelka, *J. Am. Chem. Soc.* **119**, 3596 (1997); G. S. Attard, J. C. Glyde, C. G. Göltner, *Nature* **378**, 366 (1995).
8. V. Sankaran, C. C. Cummins, R. R. Schrock, R. E. Cohen, R. J. Silbey, *J. Am. Chem. Soc.* **112**, 6858 (1990); Y. N. C. Chan, R. R. Schrock, R. E. Cohen, *Chem. Mater.* **4**, 24 (1992); M. Moffitt, L. McMahon, V. Pessel, A. Eisenberg, *ibid.* **7**, 1185 (1995); J. P. Spatz, A. Roescher, S. Sheiko, G. Krausch, M. Möller, *Adv. Mater.* **7**, 731 (1995); M. Antonietti, E. Wenz, L. Bronstein, M. Seregina, *ibid.*, p. 1000; R. T. Clay and R. E. Cohen, *Supramol. Sci.* **2**, 183 (1995); R. S. Kane, R. E. Cohen, R. Silbey, *Chem. Mater.* **8**, 1919 (1996).
9. P. V. Braun, P. Osenar, S. I. Stupp, *Nature* **380**, 325 (1996).
10. J. H. Golden *et al.*, *Science* **273**, 782 (1996).
11. J. M. Marentette, J. Norwig, E. Stöckelmann, W. H. Meyer, G. Wegner, *Adv. Mater.* **9**, 647 (1997).
12. M. A. Hillmyer *et al.*, *Science* **271**, 976 (1996).
13. F. S. Bates, *ibid.* **251**, 898 (1991).
14. H. Schmidt and H. Wolter, *J. Non-Cryst. Solids* **121**, 428 (1990).
15. J. Allgaier, A. Poppe, L. Willner, D. Richter, *Macromolecules* **30**, 1582 (1997).
16. The prehydrolyzed sol was prepared by mixing GLYMO and $Al(OBu^s)_3$ at 273 K and adding 15% of the stoichiometric amount of water required for the complete hydrolysis of the metal alkoxide groups. The water contained HCl in a molar ratio (relative to the metal alkoxides) of 3.6×10^{-5}:1. After 15 min of stirring, the temperature was raised to 295 K. After a further 15 min, the residual water for the complete hydrolysis of the alkoxide groups was added, and the mixture was stirred for 1 hour and then poured into the block copolymer solution.
17. L. Reimer, *Adv. Electron. Electron Phys.* **81**, 67 (1991).
18. M. Templin, A. Franck, A. Du Chesne, H. Leist, Y. Zhang, R. Ulrich, V. Schädler, U. Wiesner, data not shown.
19. DSC measurements were performed on a Mettler DSC-30 with a heating rate of 10 K min^{-1}. Evaluation of the DSC curves was performed with a program from the same company.
20. S. Krause, in *Polymer Blends*, D. R. Paul and S. Newman, Eds. (Academic Press, New York, 1978), vol. 1, pp. 16–113; L. Robeson, in *Polymer Compatibility and Incompatibility*, K. Solc, Ed. (MMI Press Symposium Series, Harwood Academic, New York, 1982), vol. 2, pp. 177–211.
21. M. Templin, U. Wiesner, H. W. Spiess, *Adv. Mater.* **9**, 814 (1997).
22. T. Hashimoto, K. Nagatoshi, A. Todo, H. Hasegawa, H. Kawai, *Macromolecules* **7**, 364 (1977); D. Ehlich, M. Takenaka, S. Okamoto, T. Hashimoto, *ibid.* **26**, 189 (1993); C. C. Honeker and E. L. Thomas, *Chem. Mater.* **8**, 1702 (1996).
23. Y. Liu, M. H. Rafailovich, J. Sokolov, S. A. Schwarz, S. Bahal, *Macromolecules* **29**, 899 (1996); G. Coulon, T. P. Russell, V. R. Deline, P. F. Green, *ibid.* **22**, 2581 (1989); C. S. Henkee, E. L. Thomas, L. J. Fetters, *J. Mater. Sci.* **23**, 1685 (1988).
24. A. Du Chesne, G. Lieser, G. Wegner, *Colloid Polym. Sci.* **272**, 1329 (1994); A. Du Chesne, K. Wenke, G. Lieser, G. Wenz, *Acta Polym.* **48**, 142 (1997)
25. The decrease of the lamellar spacing is exclusively attributable to convex bending of the liquid-like lamellar surface. Two driving forces must be considered: surface tension (up to a critical ratio of lamella thickness to section thickness, the free lamella surface decreases upon bending) and entropy [partial relaxation of entropically unfavorable chain conformation (stretched chains in lamellae in bulk)]. For details, see A. Du Chesne, thesis, University of Mainz (1993).

26. We thank H. W. Spiess for his strong support of this work, T. Thurn-Albrecht for help in performing SAXS measurements and for fruitful discussions, and U. Pawelzik for performing the DSC measurements. M.T. thanks the Bundesministerium für Bildung, Wissenschaft, Forschung und Technologie (project 03 N 1009C0) for financial support.

8 July 1997; accepted 23 October 1997

Promotion of the Cycling of Diet-Enhancing Nutrients by African Grazers

S. J. McNaughton,* F. F. Banyikwa, M. M. McNaughton

Experiments in Serengeti National Park, Tanzania, provide direct evidence that large, free-ranging mammalian grazers accelerate nutrient cycling in a natural ecosystem in a way that enhances their own carrying capacity. Both nitrogen and sodium were at considerably higher plant-available levels in soils of highly grazed sites than in soils of nearby areas where animal density is sparse. Fencing that uncoupled grazers and soils indicated that the animals promote nitrogen availability on soils of inherently similar fertility and select sites of higher sodium availability as well as enhancing that availability.

There is a growing recognition in ecology that organisms can modify their environments in ways beneficial to themselves, rather than inevitably causing environmental deterioration (*1*), and it is a maxim of grassland ecology that nutrient recycling by grazers contributes to plant regrowth potential (*2*). However, direct evidence of the effect of large wild mammals on nutrient recycling is meager (*3*), and studies in boreal forests (*4*) indicate that moose (*Alces alces*) browsing indirectly diminishes soil mineralization rate by shifting the composition of vegetation species to less palatable and less decomposable plants.

The distribution and abundance of large grazing mammals in Serengeti National Park, Tanzania, are influenced by the occurrence of nutritionally sufficient forages (*5*) and the spatiotemporal variation of vegetation productivity due to pronounced geographic rainfall gradients and production seasonality (*6*). Grazers preferentially forage on swards enriched in minerals that are important in late-stage pregnancy, lactation, and the growth of young animals (*5*). There are two plausible explanations for this phenomenon: Animals forage on vegetation supported by soils of innately greater nutrient availability, or animal activities augment nutrient availability. Identification of the correct explanation has implications for conservation policy and management (through an understanding of the habitat requirements of endangered wild grazing mammals) and for ecological theory (by documenting how grazing mammals are mechanistically coupled with their habitats). Regional edaphic differences affect the mineral contents of forages and thereby influence seasonal movements of migratory grazers in the Serengeti, but no evidence of general soil differences was found in landscape-level studies of resident grazers (*5*), which are those that do not migrate but occupy discrete home ranges. Here we present evidence concerning the mechanisms associated with higher nutrient availability at sites preferred by resident grazers.

Mineralization of two elements—nitrogen (N), which is essential to both plants

S. J. McNaughton and M. M. McNaughton, Biological Research Laboratories, Syracuse University, Syracuse, NY 13244–1220, USA; and Serengeti Wildlife Research Centre, Post Office Box 661, Arusha, Tanzania.
F. F. Banyikwa, Department of Botany, University of Dar es Salaam, Post Office Box 35060, Dar es Salaam, Tanzania; Biological Research Laboratories, Syracuse University, Syracuse, NY 13244–1220, USA; and Serengeti Wildlife Research Centre, Post Office Box 661, Arusha, Tanzania.

*To whom correspondence should be addressed: E-mail: sjmcnaug@mailbox.syr.edu